

# Multi-Processor Approximate Message Passing with Lossy Compression

Junan Zhu, *Student Member, IEEE*, and Dror Baron, *Senior Member, IEEE*

**Abstract**—We consider large-scale linear inverse problems in Bayesian settings. Our general approach follows a recent line of work that applies the approximate message passing (AMP) framework in multi-processor (MP) computational systems by storing and processing a subset of rows of the measurement matrix along with corresponding measurements at each MP node. In each MP-AMP iteration, nodes of the MP system and its fusion center exchange messages pertaining to their estimates of the input. Unfortunately, communicating these messages is often costly in applications such as sensor networks. To reduce the communication costs, we apply lossy compression to the messages. To improve compression, we realize that the rate distortion trade-off differs among MP-AMP iterations, and use dynamic programming (DP) to optimize per-iteration coding rates. Numerical results confirm that the proposed coding rates offer significant and often dramatic reductions in communication costs. That said, computational costs involve two matrix vector products per MP-AMP iteration, which may be significant for large matrices. Therefore, we further improve the trade-off between computational and communication costs with a modified DP scheme. Case studies involving sensor networks and large-scale computing systems highlight the potential of our approach.

**Index Terms**—approximate message passing, cloud computing, compressed sensing, dynamic programming, lossy compression, rate distortion theory, sensor networks.

## I. INTRODUCTION

Many scientific and engineering problems [2, 3] can be approximated as linear systems of the form

$$\mathbf{y} = \mathbf{A}\mathbf{x} + \mathbf{z}, \quad (1)$$

where  $\mathbf{x} \in \mathbb{R}^N$  is the unknown input signal,  $\mathbf{A} \in \mathbb{R}^{M \times N}$  is the matrix that characterizes the linear system, and  $\mathbf{z} \in \mathbb{R}^M$  is measurement noise. The goal is to estimate  $\mathbf{x}$  from the noisy measurements  $\mathbf{y}$  given  $\mathbf{A}$  and statistical information about  $\mathbf{z}$ . When  $M \ll N$ , the setup (1) is known as compressed sensing (CS) [2, 3]; by posing a sparsity or compressibility requirement on the signal, it is indeed possible to accurately recover  $\mathbf{x}$  from the ill-posed linear system [2, 3]. However, we might need  $M > N$  when the signal is dense or the noise is substantial.

### A. Background and prior art

**Multi-processor CS:** In real-world applications, a multi-processor (MP) version of CS could be of interest, due to

either storage limitations in each individual processor node, or the need for fast computation. This paper considers multi-processor CS (MP-CS) [1, 4–10], in which there are  $P$  distributed nodes (processor nodes) and a fusion center. Each distributed node stores  $\frac{M}{P}$  rows of the matrix  $\mathbf{A}$ , and acquires the corresponding linear measurements of the underlying signal  $\mathbf{x}$ . Without loss of generality, we model the measurement system in distributed node  $p \in \{1, \dots, P\}$  as

$$y_i = \mathbf{A}_i \mathbf{x} + z_i, \quad i \in \left\{ \frac{M(p-1)}{P} + 1, \dots, \frac{Mp}{P} \right\}, \quad (2)$$

where  $\mathbf{A}_i$  is the  $i$ -th row of  $\mathbf{A}$ , and  $y_i$  and  $z_i$  are the  $i$ -th entries of  $\mathbf{y}$  and  $\mathbf{z}$ , respectively. Once every  $y_i$  is collected, we run distributed algorithms among the fusion center and  $P$  distributed nodes to reconstruct the underlying signal  $\mathbf{x}$ .

**Approximate message passing (AMP):** AMP [11–13] is an iterative framework that solves linear inverse problems by successively decoupling [14–16] matrix channel problems into scalar channel denoising problems with additive white Gaussian noise (AWGN). AMP has received considerable attention, because of its fast convergence and the state evolution (SE) formalism [11, 13], which offers a precise characterization of the AWGN denoising problem in each iteration. For Gaussian  $\mathbf{A}$ , AMP with separable denoisers has been rigorously proved to obey SE [13]. In the Bayesian setting, AMP often achieves the minimum mean squared error (MMSE) [17–19] in the limit of large linear systems. In this paper, we investigate AMP tailored for MP-CS.

**Multi-processor AMP:** MP versions of AMP (MP-AMP) for MP-CS have been studied in the literature [1, 7]. MP-AMP iterates over the following two steps. First, each distributed node decouples [14–16] its own matrix channel (2) into its equivalent scalar channel with AWGN. Second, the fusion center merges all the noisy signals from the equivalent scalar channels of all distributed nodes, denoises the merged noisy signal, and transmits the denoised signal back to each distributed node. Details about MP-AMP appear in Sec. II-B.

Usually, MP platforms are designed for distributed settings such as sensor networks [20, 21] or large-scale “big data” computing systems [22]. The communication cost (power consumption) in sensor networks is high due to the limited power available to the sensors [23]. The communication cost (time) in large-scale computing systems is somewhat smaller [22]. In order to provide a reasonable trade-off between communication and computation, we reduce the communication costs of MP platforms such as sensor networks [20, 21] and large-scale computing systems [22] by applying lossy compression [24–26] to the communication portion of MP-AMP.

**Rate distortion theory:** Suppose that we want to transmit a

A subset of the work with Puxiao Han and Riuxin Niu will appear at the 41st IEEE International Conference on Acoustics, Speech and Signal Processing, Shanghai, China, Mar. 2016 [1].

The work was supported in part by the National Science Foundation under the Grant CCF-1217749 and in part by the U.S. Army Research Office under the Contract W911NF-14-1-0314.

Junan Zhu and Dror Baron are with the Department of Electrical and Computer Engineering, NC State University, Raleigh, NC 27695. E-mail: {jzhu9, barondror}@ncsu.edu.

sequence  $\mathbf{q} \in \mathbb{R}^N$ , and  $C$  bits are used to encode  $\mathbf{q}$ , resulting in a distorted version  $\hat{\mathbf{q}}$ . The *coding rate* is defined as  $R = \frac{C}{N}$ , which is the average number of bits needed to encode each entry of  $\mathbf{q}$ . The *distortion* is given by  $D = \frac{1}{N} \sum_{i=1}^N d(q_i, \hat{q}_i)$ , where  $q_i$  and  $\hat{q}_i$  are entries of  $\mathbf{q}$  and  $\hat{\mathbf{q}}$ , respectively, and  $d(q_i, \hat{q}_i) = (q_i - \hat{q}_i)^2$ .<sup>1</sup> Rate distortion (RD) theory [24–26] characterizes the fundamental information theoretic limits on the coding rate  $R$  for communicating a sequence  $\mathbf{q}$  up to distortion  $D$ . A pivotal conclusion from RD theory is that coding rates can be greatly reduced even if  $D$  is quite small.

**Dynamic programming:** According to RD theory, we can transmit data with greatly reduced coding rates, if we allow some distortion at the output. However, what is missing is how to allocate the coding rate among the distributed nodes and the fusion center in each MP-AMP iteration. In this paper, we propose to use dynamic programming (DP, cf. Bertsekas [27]) to optimize the coding rate allocation for MP-AMP. The obtained coding rates are verified to be optimal through extensive numerical results. Indeed, the savings in the coding rate are often dramatic.

### B. Synopsis of DP results

In the following, we briefly showcase some of the results of this paper. Due to the different constraints on actual MP systems, the communication cost and computational cost can be quite different [22, 23]. It is sometimes helpful to optimize combined communication and computational costs for a particular mean squared error (MSE)  $\Delta$  dB greater than the MMSE. Our results show dramatic savings in the costs for carrying out the reconstruction process. As an example, consider reconstructing a signal with 10% of entries following a Gaussian distribution with 0 mean and variance 1,  $\mathcal{N}(0, 1)$ , and the rest being 0. The signal is measured in an MP platform with  $P = 100$  distributed nodes according to (2), where the entries of the measurement matrix  $\mathbf{A}$  follow a Gaussian distribution with 0 mean and variance  $\frac{1}{M}$ ,  $\mathcal{N}(0, \frac{1}{M})$ . The *measurement rate*  $\kappa = \frac{M}{N}$  in our example is 0.4. Define the signal-to-noise ratio (SNR) as

$$\text{SNR} = 10 \log_{10} \left( \frac{\mathbb{E}(X^2)}{\kappa \sigma_Z^2} \right), \quad (3)$$

where  $X$  is the source that generates  $\mathbf{x}$  and  $\sigma_Z^2$  is the noise variance. We analyze the SNR=20 dB case for MP platforms [20–22] with various relative costs between computation and communication. Running the unconstrained DP scheme developed in Sec. VI-B, we obtain the coding rate needed to transmit the noisy signal from each distributed node to the fusion center in each MP-AMP iteration. These coding rates yield the lowest combined cost of computation and communication while helping MP-AMP achieve an MSE that is within  $\Delta \in \{0.3, 0.5, 1.0\}$  dB of the MMSE. Denote the resulting coding rate at iteration  $t$  by  $R_t$ ,  $t = 1, \dots, T$ , where  $T$  is the total number of MP-AMP iterations needed. In Fig. 1, we plot the aggregate coding rate,

$$R_{agg} = \sum_{t=1}^T R_t, \quad (4)$$

<sup>1</sup>Other distortion metrics  $d(\cdot, \cdot)$  can also be used [25].

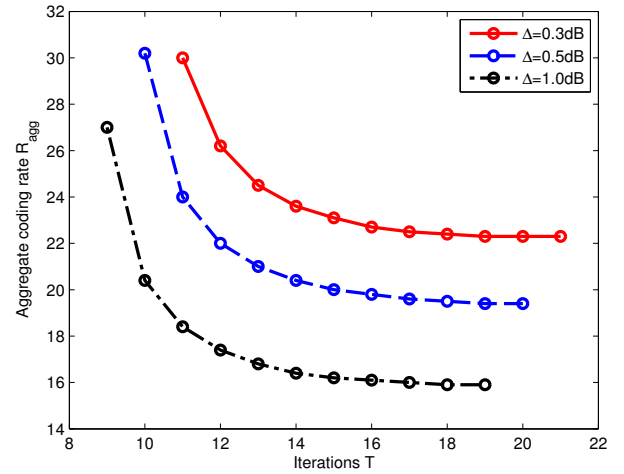


Fig. 1. Optimal aggregate coding rate  $R_{agg}$  (4) versus MP-AMP iterations  $T$  provided by unconstrained DP (cf. Sec. VI-B) under a variety of trade-offs between communication and computational costs. The signal being reconstructed has 10% entries following a Gaussian distribution, and the rest being zero. The setting is: measurement rate  $\kappa = \frac{M}{N} = 0.4$ ,  $P = 100$  distributed nodes, and SNR=20 dB (3). Different curves correspond to final MSE's that are  $\Delta \in \{0.3, 0.5, 1.0\}$  dB above the MMSE.

over the entire reconstruction process as a function of  $T$  for different  $\Delta$ . Indeed, different trade-offs between computation and communication can lead to different aggregate coding rates  $R_{agg}$  and numbers of MP-AMP iterations  $T$ . The properties of the curves in Fig. 1 are studied in detail in Sec. VI-D.

### C. Organization

The rest of the paper is organized as follows. Sec. II provides background content. Sec. III formulates a DP scheme that achieves the smallest MSE with a given budget for the number of iterations  $T$  and aggregate coding rate  $R_{agg}$  (4). Sec. IV presents a practical design for the quantizer used in the DP scheme of Sec. III. Sec. V demonstrates numerically that the DP-predicted MSE can be achieved through MP-AMP, and that the savings in coding rates are often dramatic with the MSE being only marginally worse than the MMSE. Sec. VI extends the DP scheme of Sec. III to practical problems and obtains coding rates that minimize the actual physical costs in a variety of cases, and Sec. VII concludes the paper and proposes some topics for future work.

## II. BACKGROUND

### A. Centralized CS using AMP

In the linear system (1), we consider an independent and identically distributed (i.i.d.) Gaussian measurement matrix  $\mathbf{A}$ , i.e.,  $\mathbf{A}_{i,j} \sim \mathcal{N}(0, \frac{1}{M})$ . The signal entries follow an i.i.d. *Bernoulli Gaussian* distribution,

$$x_j \sim \epsilon \mathcal{N}(0, 1) + (1 - \epsilon) \delta(x_j), \quad (5)$$

where  $\delta(\cdot)$  is the Dirac delta function and  $\epsilon$  is called the *sparsity rate* of the signal. The noise entries obey  $z_i \sim \mathcal{N}(0, \sigma_Z^2)$ , where  $\sigma_Z^2$  is the noise variance. Note that the results in this paper can be easily extended to priors other than (5).

Starting from  $\mathbf{x}_0 = \mathbf{0}$ , the AMP framework [11] proceeds iteratively according to

$$\mathbf{x}_{t+1} = \eta_t(\mathbf{A}^\mathcal{T} \mathbf{r}_t + \mathbf{x}_t), \quad (6)$$

$$\mathbf{r}_t = \mathbf{y} - \mathbf{A} \mathbf{x}_t + \frac{1}{\kappa} \mathbf{r}_{t-1} \langle d\eta_{t-1}(\mathbf{A}^\mathcal{T} \mathbf{r}_{t-1} + \mathbf{x}_{t-1}) \rangle, \quad (7)$$

where  $t$  represents the iteration index,  $\mathcal{T}$  denotes transpose,  $\kappa = \frac{M}{N}$ ,  $\eta_t(\cdot)$  is a denoising function, and  $\langle \mathbf{u} \rangle = \frac{1}{N} \sum_{i=1}^N u_i$  for some vector  $\mathbf{u} \in \mathbb{R}^N$ . The denoising function  $\eta_t(\cdot)$  is separable in the original derivation of AMP [11–13]. That is,  $\eta_t(\mathbf{u}) = (\eta_t(u_1), \eta_t(u_2), \dots, \eta_t(u_N))$  and  $d\eta_t(\mathbf{u}) = (d\eta_t(u_1), d\eta_t(u_2), \dots, d\eta_t(u_N))$ , where  $d\eta_t(\cdot) = \frac{d\eta_t(\cdot)}{d\{\cdot\}}$  is shorthand for the derivative of  $\eta_t(\cdot)$ . Owing to the decoupling effect [14–16], in each AMP iteration [12, 13], the vector  $\mathbf{f}_t = \mathbf{A}^\mathcal{T} \mathbf{r}_t + \mathbf{x}_t$  in (6) is statistically equivalent to the input signal  $\mathbf{x}$  corrupted by AWGN  $\mathbf{w}_t$  generated by a source  $W \sim \mathcal{N}(0, \sigma_t^2)$ ,

$$\mathbf{f}_t = \mathbf{x} + \mathbf{w}_t. \quad (8)$$

A useful property of AMP [12, 13] is that the noise variance  $\sigma_t^2$  evolves following state evolution (SE) in the limit of large systems ( $N \rightarrow \infty, \frac{M}{N} \rightarrow \kappa$ ):

$$\sigma_{t+1}^2 = \sigma_Z^2 + \frac{1}{\kappa} \text{MSE}(\eta_t, \sigma_t^2). \quad (9)$$

In (9),  $\text{MSE}(\eta_t, \sigma_t^2) = \mathbb{E}_{X,W} [(\eta_t(X+W) - X)^2]$ , where  $\mathbb{E}_{X,W}(\cdot)$  is expectation with respect to  $X$  and  $W$ , and  $X \sim f_X$  is the source that generates  $\mathbf{x}$ . Note that  $\sigma_1^2 = \sigma_Z^2 + \frac{\mathbb{E}[X^2]}{\kappa}$ , because of the all-zero initial estimate for  $\mathbf{x}$ . Formal statements for SE appear in [12, 13]. Additionally, it is convenient to use the following estimator for  $\sigma_t^2$  [12, 13]:

$$\hat{\sigma}_t^2 = \frac{1}{M} \|\mathbf{r}_t\|_2^2, \quad (10)$$

where  $\|\cdot\|_2$  denotes the  $\ell_2$  norm.

In this paper, we confine ourselves to the Bayesian setting, in which we assume knowledge of the true prior for the signal  $\mathbf{x}$ . Therefore, the MMSE-achieving denoiser is the conditional expectation,  $\eta_t(\cdot) = \mathbb{E}[\mathbf{x}|\mathbf{f}_t]$ , which is explicitly given in (11) for Bernoulli Gaussian signals (5),

$$\eta_t(f_{t,i}) = \frac{\epsilon}{\epsilon + (1-\epsilon)\sqrt{1 + \frac{1}{\sigma_t^2} \exp\left[-\frac{f_{t,i}^2}{2\sigma_t^2(1+\sigma_t^2)}\right]}} \cdot \frac{f_{t,i}}{1 + \sigma_t^2}, \quad (11)$$

where  $f_{t,i}$  is the  $i$ -th entry of  $\mathbf{f}_t$ . The derivative of  $\eta_t(f_{t,i})$  (11) can be easily obtained, and is omitted for brevity. Other denoisers such as soft thresholding [11–13] yield MSE's that are greater than that of the Bayesian denoiser (11). When the true prior for  $\mathbf{x}$  is unavailable, parameter estimation techniques can be used; we leave their study for future work.

## B. MP-CS using MP-AMP

In the sensing problem formulated in (2), the measurement matrix is stored in a distributed manner in each distributed

node. MP-AMP [1, 7] iteratively solves MP-CS problems:

$$\text{Distributed nodes: } \mathbf{r}_t^p = \mathbf{y}^p - \mathbf{A}^p \mathbf{x}_t + \frac{1}{\kappa} \mathbf{r}_{t-1}^p g_{t-1}, \quad (12)$$

$$\mathbf{f}_t^p = \frac{1}{P} \mathbf{x}_t + (\mathbf{A}^p)^\mathcal{T} \mathbf{r}_t^p, \quad (13)$$

$$\text{Fusion center: } \mathbf{f}_t = \sum_{p=1}^P \mathbf{f}_t^p, \quad (14)$$

$$g_t = \langle d\eta_t(\mathbf{f}_t) \rangle, \quad (15)$$

$$\mathbf{x}_{t+1} = \eta_t(\mathbf{f}_t). \quad (16)$$

Note that (12)–(13) are computed in distributed nodes, and (14)–(16) are carried out at the fusion center.

An MP-AMP iteration refers to the process from (12) to (16). We can see that there are two routes to transmit data, (i) *uplink*: distributed nodes transmit  $\mathbf{f}_t^p, \forall p \in \{1, \dots, P\}$ , to the fusion center and (ii) *downlink*: the fusion center transmits the denoised signal vector  $\mathbf{x}_t$  and a scalar  $g_{t-1}$  to the distributed nodes. The transmission of the scalar  $g_{t-1}$  is negligible, and the fusion center may broadcast  $\mathbf{x}_t$  so that naive compression of  $\mathbf{x}_t$  is sufficient. Hence, in this paper we will not focus on possible lossy compression of the downlink, and will only focus on lossy compression schemes for the uplink. The proposed DP schemes in Secs. III and VI can be easily adapted to optimize the downlink as well.

## C. Rate distortion theory and lossy MP-AMP

In lossy compression, using reduced coding rates to transmit a signal will incur larger distortion. Formally, the rate distortion function, denoted by  $R(D)$ , offers the fundamental information theoretic limit on the coding rate  $R$  for communicating a sequence  $\mathbf{q}$  up to distortion  $D$  [24–26]. The function  $R(D)$  can be computed in various ways [28–30], and can be achieved by an RD-optimal quantization scheme. Other quantization schemes require larger coding rates to achieve the same expected distortion  $D$ .

Applying lossy compression to the uplink of MP-AMP, we must quantize  $\mathbf{f}_t^p, \forall p$ , and encode the quantized vector  $Q(\mathbf{f}_t^p)$  instead. We incur a distortion (or quantization error)  $D_t^p = \frac{1}{N} \sum_{i=1}^N (Q(f_{t,i}^p) - f_{t,i}^p)^2$  at iteration  $t$  in each distributed node, where  $Q(f_{t,i}^p)$  and  $f_{t,i}^p$  are the  $i$ -th entries of the vectors  $Q(\mathbf{f}_t^p)$  and  $\mathbf{f}_t^p$ , respectively. Because we assume that the measurement matrix  $\mathbf{A}$  and noise  $\mathbf{z}$  are both i.i.d., the expected distortions  $D_t^p$  are the same over all  $P$  distributed nodes, and can be denoted by  $D_t$  for simplicity. We can model the quantization process as  $Q(\mathbf{f}_t^p) = \mathbf{f}_t^p + \mathbf{n}_t^p$ , where entries of  $\mathbf{n}_t^p$  are i.i.d. additive quantization error with zero mean and variance  $D_t$ . One technique to approach the RD function is vector quantization (VQ) [26, 31, 32] in the limit of long blocks,<sup>2</sup> where the quantization error can be modeled as i.i.d. Gaussian,  $\mathbf{n}_t^p \sim \mathcal{N}(0, D_t \mathbb{I}_N)$ , with  $\mathbb{I}_N$  representing an identity matrix of size  $N \times N$ . Moreover,  $\mathbf{n}_t^p$  is independent of the original signal  $\mathbf{f}_t^p$  being quantized.

In the remainder of Sec. II, we assume that appropriate VQ schemes that achieve  $R(D)$  are applied within each MP-AMP iteration. Therefore, we can model the signal at each

<sup>2</sup>VQ partitions the sequence into blocks, and each block is mapped to bits [26, 31, 32].

distributed node after quantization as

$$\begin{aligned} Q(\mathbf{f}_t^p) &= \frac{1}{P} \mathbf{x}_t + (\mathbf{A}^p)^T \mathbf{r}_t^p + \mathbf{n}_t^p \\ &= \frac{1}{P} \mathbf{x} + \mathbf{w}_t^p + \mathbf{n}_t^p, \end{aligned} \quad (17)$$

where (17) is due to the equivalent scalar channel discussed in (8) [14, 33]. The equivalent scalar channel noise in distributed node  $p$  is  $\mathbf{w}_t^p \sim \mathcal{N}(0, \frac{\sigma_t^2}{P} \mathbb{I}_N)$  with  $\sum_{p=1}^P \mathbf{w}_t^p = \mathbf{w}_t$  (cf. (8)). We call

$$\mathbf{v}_t^p = \mathbf{w}_t^p + \mathbf{n}_t^p \quad (18)$$

the *overall discrepancy* in distributed node  $p$ . Note that  $\mathbf{v}_t^p \sim \mathcal{N}(0, (\frac{\sigma_t^2}{P} + D_t) \mathbb{I}_N)$  due to the use of VQ schemes that achieve  $R(D)$ . The signal at the fusion center before denoising can be modeled as

$$\mathbf{f}_{Q,t} = \sum_{p=1}^P Q(\mathbf{f}_t^p) = \mathbf{x} + \mathbf{w}_t + \mathbf{n}_t = \mathbf{x} + \mathbf{v}_t, \quad (19)$$

where  $\mathbf{w}_t \sim \mathcal{N}(0, \sigma_t^2 \mathbb{I}_N)$  is the equivalent scalar channel noise and  $\mathbf{n}_t = \sum_{p=1}^P \mathbf{n}_t^p$  is the overall quantization error. We call

$$\mathbf{v}_t = \sum_{p=1}^P \mathbf{v}_t^p \quad (20)$$

the overall discrepancy at the fusion center. Because  $\mathbf{f}_t^p$  is compressed lossily, the signal processed by the denoiser in (15) and (16) becomes  $\mathbf{f}_{Q,t}$ .<sup>3</sup> Also, the SE for the lossily compressed  $\mathbf{f}_t^p$  must be modified,

$$\sigma_{t+1}^2 = \sigma_Z^2 + \frac{1}{\kappa} \text{MSE}(\eta_t, \sigma_t^2 + PD_t), \quad (21)$$

where we remind the reader that  $\sigma_t^2$  can be estimated by (10), and  $\sigma_{t+1}^2$  is the variance of  $\mathbf{w}_{t+1}$  (19).

Recall from Sec. I-B that  $R_t$  is the coding rate used to transmit  $\mathbf{f}_t^p$  at iteration  $t$ . The sequence of  $R_t$ ,  $t = 1, \dots, T$ , where  $T$  is the total number of MP-AMP iterations, is called the *coding rate sequence*, and is denoted by  $(R_t)$ . Given the coding rate sequence  $(R_t)$ , the distortion  $D_t$  can be evaluated with  $R(D)$ , and the scalar channel noise variance  $\sigma_t^2$  can be evaluated with (21). Hence, the MSE for  $(R_t)$  can be predicted; we call it DP-predicted MSE.

In general, there is no closed form for  $R(D)$ , and it is computed by algorithms such as Blahut-Arimoto [28, 29]. Nevertheless,  $R(D)$  can be bounded by the Shannon lower bound (SLB) [25] as  $R(D) \geq h(X) - h(D)$ , where  $h(X)$  and  $h(D)$  are the differential entropy [25] of the input source  $X$  and a Gaussian source with zero mean and variance  $D$ , respectively. Fortunately, when a reverse channel from the output to the input can be identified, the SLB is tight [25], and  $R(D) = h(X) - h(D)$ . In our case, the source  $\mathbf{f}_t^p$  can be approximated as  $\frac{1}{P} \mathbf{x} + \mathbf{w}_t^p$  that follows

$$\mathbf{f}_t^p \sim \epsilon \mathcal{N}\left(0, \left(\frac{1}{P^2} + \frac{\sigma_t^2}{P}\right) \mathbb{I}_N\right) + (1 - \epsilon) \mathcal{N}\left(0, \frac{\sigma_t^2}{P} \mathbb{I}_N\right). \quad (22)$$

Therefore, the reverse channel can be identified when  $D_t \leq$

$\frac{\sigma_t^2}{P}$ , in which case  $R(D)$  is obtained from the SLB. When  $D_t > \frac{\sigma_t^2}{P}$ , the SLB is loose and  $R(D)$  is calculated using other algorithms such as Blahut-Arimoto [28, 29].

### III. DYNAMIC PROGRAMMING

Following the discussion of Sec. II, we can see that compressing  $\mathbf{f}_t^p, \forall p \in \{1, \dots, P\}$ , lossily (17) can reduce communication costs. The aggregate coding rate  $R_{agg}$  (4) is the sum of the coding rates used to transmit  $\mathbf{f}_t^p$  among all MP-AMP iterations. The greater the savings in the aggregate coding rate (4), the worse the final MSE is expected to be. With this in mind, we formally state the following question: *For a given aggregate coding budget  $R_{agg}$  (4), total number of MP-AMP iterations  $T$ , and initial noise level  $\sigma_1^2$  in the scalar channel (19),<sup>4</sup> what is the coding rate sequence  $(R_t)$  that minimizes the final MSE?*

**Derivation of DP scheme:** To answer the question above, we derive a dynamic programming (DP) [27] scheme. We first define the remaining aggregate coding rate  $R_{rem}(t)$  as

$$R_{rem}(t) = R_{agg} - \sum_{\tilde{t}=1}^t R'_{\tilde{t}}, \quad (23)$$

where  $R'_{\tilde{t}}, \tilde{t} = 1, \dots, t$ , are the coding rates used to transmit  $\mathbf{f}_{\tilde{t}}^p$  in the first  $t$  MP-AMP iterations. We then define the cost function  $\Psi_{T-t}(R_{rem}(t), \sigma_t^2)$  as the lowest MSE achieved among all coding rate sequences whose aggregate coding rate is  $R_{rem}(t)$  with  $(T - t)$  remaining iterations, where  $\sigma_t^2$  is the variance of the noise  $\mathbf{w}_t$  of (19) at MP-AMP iteration  $t$ .

The lowest MSE  $\Psi_{T-t}(R_{rem}(t), \sigma_t^2)$  is computed using standard dynamic programming (DP) methods [27]. The basis case of DP involves  $T - t = 0$ , meaning that we are in the last iteration and compress using the entire remaining coding rate  $R_{rem}(t)$ ,  $t = T$ . Since we do not know  $R_{rem}(T)$  and  $\sigma_T^2$  in advance, we calculate  $\Psi_0(R_{rem}(T), \sigma_T^2)$  for every possible  $R_{rem}(T)$  and  $\sigma_T^2$ , and store the results (additional details appear in the Appendix). Next, we iterate back in time by decreasing  $t$  (equivalently, increasing  $T - t$ ),

$$\Psi_{T-t}(R_{rem}(t), \sigma_t^2) = \min_{R'} \Psi_{T-(t+1)}(R_{rem}(t+1), \sigma_{t+1}^2(R')) \quad (24)$$

for every possible  $R_{rem}(t)$  and  $\sigma_t^2$ , where  $R'$  is the coding rate used in the current MP-AMP iteration  $t$ . Note that  $R_{rem}(t+1) = R_{rem}(t) - R'$  is the remaining aggregate coding rate left for all future iterations  $t+1, \dots, T$ , after using a coding rate  $R'$  in the current iteration  $t$ . Furthermore,  $\sigma_{t+1}^2(R')$  is the variance of the noise  $\mathbf{w}_{t+1}$  of the scalar channel (19) in MP-AMP iteration  $(t+1)$  after transmitting the current  $\mathbf{f}_t^p$  at rate  $R'$ . The calculation of  $\sigma_{t+1}^2(R')$  depends on (21) and the relation between rate and distortion. In this section, we use the RD function (Sec. II-C).

The coding rates  $R'$  that minimize the cost function  $\Psi_{T-t}(R_{rem}(t), \sigma_t^2)$  for different  $t, R_{rem}(t)$  (23), and  $\sigma_t^2$  are stored in a table  $\mathcal{R}(t, R_{rem}(t), \sigma_t^2)$ . After DP finishes, we obtain the coding rate for the first MP-AMP iteration as  $R_1 = \mathcal{R}(1, R_{agg}, \sigma_Z^2 + \frac{1}{\kappa} \mathbb{E}[X^2])$ . Using  $R_1$ , we calculate  $\sigma_t^2$

<sup>3</sup>For brevity, we do not re-list the steps at the fusion center.

<sup>4</sup>As a reminder,  $\sigma_1^2 = \sigma_Z^2 + \frac{1}{\kappa} \mathbb{E}[X^2]$ .

from (21) for  $t = 2$  and  $R_{rem}(2) = R_{agg} - R_1$ , so that we find  $R_2 = \mathcal{R}(2, R_{rem}(2), \sigma_2^2)$ . Iterating from  $t = 1$  to  $T$ , we obtain the coding rate sequence  $(R_t)$ .

This DP scheme is expected to yield the optimal coding rate sequence for a given  $R_{agg}$  and  $T$ . Moreover, this DP scheme can be computationally efficient if  $\Psi_{T-(t+1)}(\cdot, \cdot)$  on the right hand side of (24) has been calculated and stored. Nevertheless, the actual search space for  $\sigma_{\cdot}^2$  and  $R_{rem}(\cdot)$  is continuous, where the subscript  $\{\cdot\}$  denotes arbitrary iteration numbers, and we cannot compute and store  $\Psi_{T-(t+1)}(R_{rem}(t+1), \sigma_{t+1}^2)$  for all continuous valued  $\sigma_{t+1}^2$  and  $R_{rem}(t+1)$ . Therefore, to be computationally tractable, the proposed DP scheme should operate in a discretized search space over  $\sigma_{\cdot}^2$  and  $R_{rem}(\cdot)$ . Denote the discretized grid of  $\sigma_{\cdot}^2$  by  $\mathcal{G}(\sigma^2) = \{\sigma_{min}^2, \sigma_{min}^2 + \Delta\sigma^2, \dots, \sigma_{max}^2\}$ , where  $\sigma_{min}^2, \sigma_{max}^2$ , and  $\Delta\sigma^2$  are the lower limit, upper limit, and resolution of the search space for  $\sigma_{\cdot}^2$ , respectively. Denote the discretized grid of  $R_{rem}(\cdot)$  by  $\mathcal{G}(R) = \{R_{min}, R_{min} + \Delta R, \dots, R_{max}\}$ , where  $R_{min}, R_{max}$ , and  $\Delta R$  are the lower limit, upper limit, and resolution of the search space for  $R_{rem}(\cdot)$ , respectively. We choose  $\Delta\sigma^2 = 0.1$  dB and  $\Delta R = 0.1$ , which we verify to yield errors smaller than 0.01 dB. Details about the resolution of our two grids and how we verify the optimality of our DP scheme appear in the Appendix.

#### IV. TOWARD PRACTICAL LOSSY COMPRESSION DESIGN

In Sec. III, we presented results for the DP scheme based on the RD function,  $R(D)$ , which can be approached in practice using vector quantization (VQ) [26, 31, 32]. Recall that VQ partitions the sequence into blocks, and maps each block into bits. To approach the RD function, the blocks must be long, which may be difficult to implement and require plenty of computation. These challenges make VQ less practical. Instead, after having provided best-possible results computed with DP using the RD function in Sec. III, this section explores a more practical alternative. We use scalar quantizers followed by entropy coding (ECSQ) [25, 26], which approaches  $R(D)$  within 0.255 bits in the high rate limit and corresponds to small  $D$  [26]. Another implementable direction for MP-AMP involves polar codes [34], but they are designed primarily for binary channels, and it is less clear how to apply them to the Gaussian channel implicit in our compression problem. Exploring how to approach the RD function in MP-AMP is left for future work.

**DP scheme with ECSQ:** In the proposed DP scheme, the key step is to obtain the distortion  $D$  from a given  $R$  or vice-versa. We can then use (21) to predict the scalar channel noise variance for the next MP-AMP iteration. The DP scheme in Sec. III used the RD function to obtain the relation between  $R$  and  $D$ ; we call this DP-RD. For ECSQ, the scalar quantizer maps the continuous valued vector  $\mathbf{f}_t^p$  to the closest among the representation levels,  $\{\dots, -2\gamma, -\gamma, 0, \gamma, 2\gamma, \dots\}$ , where  $\gamma$  is the *bin size* of the quantizer. Varying the quantizer bin size  $\gamma$  yields different distortion levels  $D$  and corresponding coding rates  $R$ ; expressions for  $R(\gamma)$  and  $D(\gamma)$  are easily computed [24–26]. We refer to the DP scheme based on ECSQ as DP-ECSQ. We verify the integrity and optimality of DP-ECSQ in the Appendix. Details are omitted for brevity.

Recall that ECSQ needs a coding rate of 0.255 bits per element above the RD function to achieve the same distortion  $D$  in the high rate limit (hence, small  $D$ ) [26]. Suppose that DP-RD optimizes over an aggregate coding rate (4)  $R_{RD}$ . We run DP-ECSQ with greater aggregate coding rate (4),  $R_{ECSQ} = R_{RD} + 0.255T$ , and compare  $\text{SDR}_{ECSQ}$ , the signal-to-distortion ratio obtained by DP-ECSQ, to  $\text{SDR}_{RD}$ , where the signal-to-distortion ratio (SDR) is defined as

$$\text{SDR} = 10 \log_{10} \left( \frac{\mathbb{E}[X^2]}{\text{MSE}} \right). \quad (25)$$

In order to compare  $\text{SDR}_{ECSQ}$  with  $\text{SDR}_{RD}$  in a comprehensive way, we consider the settings given by the Cartesian product of the following variables: (i) the number of distributed nodes  $P \in \{30, 100\}$ , (ii) sparsity rate  $\epsilon \in \{0.03, 0.1\}$ , (iii) measurement rate  $\kappa \in \{3\epsilon, 5\epsilon\}$ , (iv) total number of MP-AMP iterations  $T \in \{7, 10\}$ , (v) aggregate coding rate  $R_{agg} \in \{1.5T, 2.5T\}$ , and (vi) SNR  $\in \{10, 15\}$  dB. In total, there are 64 different settings.

Denote  $\Theta_1 = \text{SDR}_{RD} - \text{SDR}_{ECSQ}$ . Although the resulting coding rate sequence for ECSQ,  $(R_t)_{ECSQ}$ , is not  $(R_t)_{RD} + 0.255$ , because  $(R_t)_{ECSQ}$  is typically small and the 0.255 extra rate above  $R(D)$  is in the high rate limit, our numerical results (omitted for brevity) show that  $|\Theta_1| < 0.05$  dB for most of the 64 settings. The mean, median, and largest  $\Theta_1$  are 0.02 dB, 0.01 dB, and 0.21 dB, respectively.

Let us study another sequence  $(\hat{R}_t) = (R_t)_{RD} + 0.255$ . Using  $(\hat{R}_t)$  with ECSQ within MP-AMP, we can predict the resulting reconstruction quality  $\text{SDR}_{\hat{RD}}$  using (21). Similar to before, denote  $\Theta_2 = \text{SDR}_{RD} - \text{SDR}_{\hat{RD}}$ . Our numerical results (omitted for brevity) show that  $|\Theta_2| < 0.2$  dB for most of the 64 settings; the mean, median, and largest  $\Theta_2$  are 0.05 dB, 0.02 dB, and 0.32 dB, respectively. Therefore, although not optimal, given 0.255T greater aggregate coding rate, DP-ECSQ can achieve a similar final SDR to that of DP-RD.

**Non-Gaussian overall discrepancy  $\mathbf{v}_t$  (20) after ECSQ:** We use a Bayesian denoiser to reduce the overall discrepancy  $\mathbf{v}_t$  (20), under the assumption that  $\mathbf{v}_t$  resembles AWGN. However, we now explain that  $\mathbf{v}_t$  may be non-Gaussian. Recall that the signal after quantization  $Q(\mathbf{f}_t^p)$  in (17) consists of  $\frac{1}{P}\mathbf{x}$ , the AMP equivalent scalar channel noise  $\mathbf{w}_t^p$ , and the quantization error  $\mathbf{n}_t^p$ . The overall discrepancies in each distributed node and at the fusion center are given by (18) and (20), respectively. The noise  $\mathbf{w}_t^p$  is Gaussian due to the decoupling effect [14, 33, 35, 36], which AMP benefits from [11, 13], and  $\mathbf{n}_t^p$  is Gaussian and independent of  $\mathbf{w}_t^p$  for VQ (cf. Sec. II-C and Cover et. al. [25]). For ECSQ, the quantization error  $\mathbf{n}_t^p$  in each node can often be approximated as uniformly distributed, *if the signal being quantized has enough entries to be quantized to different levels*. However, the quantization error  $\mathbf{n}_t^p$  is not independent of  $\mathbf{w}_t^p$ . For low coding rates, ECSQ yields a large quantizer bin size  $\gamma$  that ends up quantizing most entries of  $\mathbf{f}_t^p$  to zero. Hence,  $\mathbf{n}_t^p$  is negatively correlated with  $\mathbf{w}_t^p$ , and the overall discrepancy (18),  $\mathbf{v}_t^p = \mathbf{w}_t^p + \mathbf{n}_t^p$ , in each distributed node is non-Gaussian.

Examples of non-Gaussian  $\mathbf{v}_t^p$  and  $\mathbf{v}_t$  are illustrated in two histograms in Fig. 2. The underlying signal  $\mathbf{x}$  follows (5) with  $\epsilon = 0.1$ ,  $P = 100$ ,  $N = 20,000$ ,  $\kappa = 0.3$ , and SNR=10

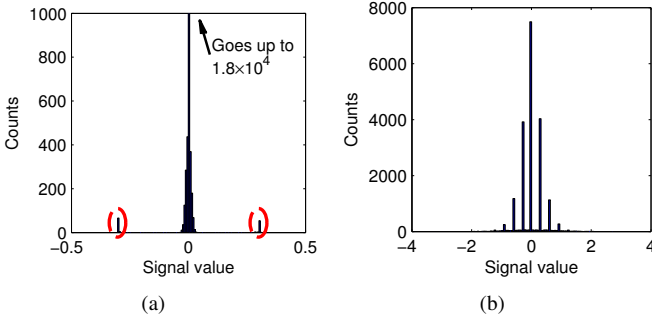


Fig. 2. Histograms of (a) the overall discrepancy  $\mathbf{v}_t^p$  (18) in a certain distributed node and (b) the overall discrepancy  $\mathbf{v}_t$  (20) at the fusion center.

dB. The quantizer in each distributed node has a bin size  $\gamma$  that is larger than the standard deviation of  $\mathbf{w}_t^p$ , which is  $\frac{\sigma_t}{\sqrt{P}}$ . Considering (22), most entries of  $\mathbf{f}_t^p$  are quantized to 0, leading to a quantization error that is negatively correlated with  $\mathbf{f}_t^p$ . Nevertheless,  $\mathbf{v}_t^p$  (18) occasionally has large magnitude in the AMP equivalent scalar channel after quantization (see the marked areas in Fig. 2(a)) for each distributed node (17). Because of the large entries in  $\mathbf{v}_t^p$ , the overall discrepancy  $\mathbf{v}_t$  (20) at the fusion center will have spikes in the histogram as shown in Fig. 2(b), after summing over the quantized data  $Q(\mathbf{f}_t^p)$  from all  $P$  nodes (19). At the fusion center (19), the denoiser estimates  $\mathbf{x}$  by removing the overall discrepancy  $\mathbf{v}_t$  (20). However,  $\mathbf{v}_t$  with a spiky histogram (Fig. 2(b)) is mismatched with respect to the distribution assumed by the Bayesian denoiser in (11) [37], making it difficult to predict the MSE after denoising. In the end, this mismatch makes the DP prediction imprecise.

In order to avoid the negative correlation between  $\mathbf{w}_t^p$  and  $\mathbf{n}_t^p$ , we must ensure that the scalar quantizer bin size is small enough, so that the noise  $\mathbf{w}_t^p$  in each distributed node is more likely to be quantized to nonzero levels. In the fusion center, the nonzero levels will make the overall noise at the fusion center appear to be Gaussian. Therefore, we constrain the bin size to be  $\gamma \leq \frac{2\sigma_t}{\sqrt{P}}$ , inspired by Widrow and Kollár [38]. Note that the constraint  $\gamma \leq \frac{2\sigma_t}{\sqrt{P}}$  is verified by the simulation described below. Other constraints may also work.

In order to verify that the constraint  $\gamma \leq \frac{2\sigma_t}{\sqrt{P}}$  effectively makes the DP-predicted SDR (25) match the MP-AMP simulated SDR in each MP-AMP iteration, we run DP-ECSQ with the constraint on the quantizer bin size  $\gamma \leq \frac{2\sigma_t}{\sqrt{P}}$  over the 64 different settings mentioned in this section. After obtaining the coding rate sequences ( $R_t$ ) for each of the 64 settings, we run MP-AMP simulations using the obtained coding rate sequences ( $R_t$ ) to reconstruct 150 signals of length 20,000 independently generated with (5). We record and plot the probability  $\Pr(\max_{t \in [1, T]} (\Delta \text{SDR}_t) \geq \xi)$  in Fig. 3, where  $\Delta \text{SDR}_t$  is the discrepancy between the mean SDR in the MP-AMP simulation and the DP-predicted SDR at iteration  $t$ , and  $\xi$  is a threshold. The result without bin size constraints is also plotted. We can see that constrained MP-AMP has a discrepancy exceeding 0.3 dB only with a negligible probability; without a constraint, even a 2 dB discrepancy occurs with probability 23%, and a 4 dB discrepancy occurs with probability 3%.

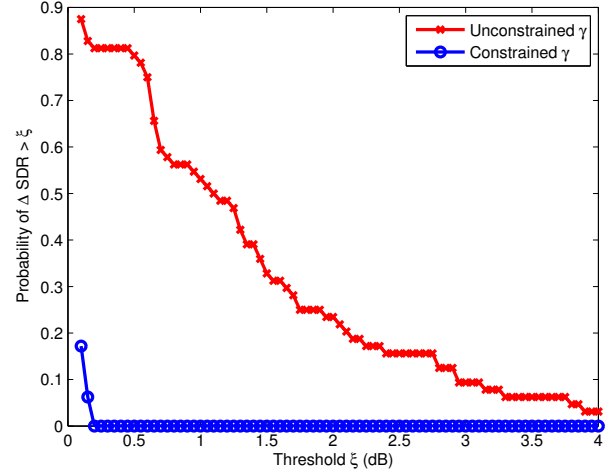


Fig. 3. Probability of  $\Delta \text{SDR}$  exceeding a threshold  $\xi$ .

The reader can see that Bayesian denoisers require to constrain the quantizer bin size  $\gamma$ . Another option is to design denoisers for spiky pdf's as in Fig. 2(b), and the quantizer bin size constraint can be removed. That said, this issue of non-Gaussian scalar channel noise is caused by ECSQ. If VQ is used, the quantization error  $\mathbf{n}_t^p$  should be independent of the quantized signal  $Q(\mathbf{f}_t^p)$  (17) and the overall discrepancy at the fusion center  $\mathbf{v}_t$  (20) should resemble i.i.d. Gaussian (19), so that the denoiser (11) achieves the MMSE.

## V. NUMERICAL RESULTS

In this section, we will use ECSQ as our lossy compression technique. To avoid the non-Gaussian  $\mathbf{v}_t$  discussed above, we constrain the quantizer bin size to  $\gamma \leq \frac{2\sigma_t}{\sqrt{P}}$  (cf. Sec. IV). We will show that DP optimized coding rate sequences can achieve an MSE that is close to the MMSE with a much lower coding rate. We will also show that an MP-AMP simulation that uses the coding rate sequence provided by DP follows the predicted SDR given by (21).

### A. MP-AMP with DP scheme

To illustrate that the DP-predicted SDR (25) can be achieved by MP-AMP that uses coding rate sequences provided by DP, we generate 50 signals of length 20,000 according to (5), and reconstruct each one by running 10 MP-AMP iterations.<sup>5</sup> The sparsity rate is  $\epsilon = 0.1$ , and  $M = 10,000$  measurements are spread over  $P = 100$  distributed nodes. Instead of transmitting the original  $\mathbf{f}_t^p$  from the distributed nodes to the fusion center, we transmit the ECSQ-quantized version of  $\mathbf{f}_t^p$  that achieves the coding rate  $R_t$  provided by DP in each MP-AMP iteration. A Bayesian denoiser (11) is used in (16).

The empirical SDR's at each MP-AMP iteration are averaged over the 50 signals, and plotted in Fig. 4 along with SDR's predicted by DP-ECSQ. We can see that the empirical SDR's at all MP-AMP iterations are close to the DP-predicted SDR. Note that the first few iterations of the solid and dashed

<sup>5</sup>The MP-AMP framework was presented in (12) – (16).



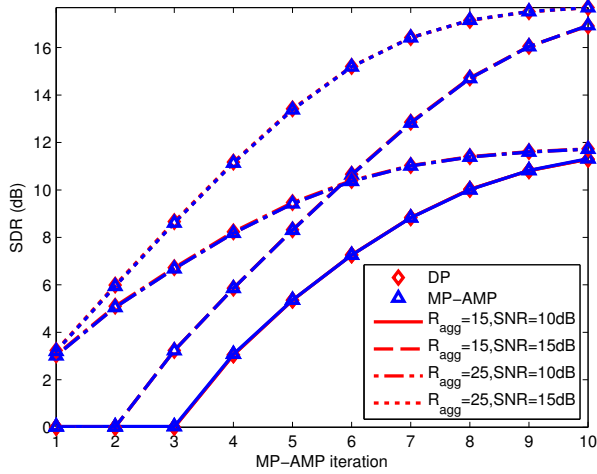


Fig. 4. Comparison of per-iteration DP-predicted SDR and the mean SDR of MP-AMP simulations for various  $R_{agg}$  (4) and SNR's.

curves have zero SDR, because DP yields a zero coding rate, in which case the distributed nodes do not transmit to the fusion center. As a result, the fusion center generates an all-zero estimate for  $\mathbf{x}_t$ , which leads to a zero SDR. The zero rates during the first few iterations are caused by the insufficient rate budget  $R_{agg}$  (4) compared to  $T$ .

### B. Achieving MMSE in various settings

The previous subsection illustrates that MP-AMP can achieve the DP-predicted SDR (25) at each iteration. In this subsection, we verify for a variety of settings that the SDR at the last iteration of MP-AMP matches the DP prediction. We also examine the difference between the MMSE<sup>6</sup> given by centralized SE (9) and the MSE provided by DP with limited MP-AMP iterations  $T$  and limited aggregate coding rate  $R_{agg}$  (4). We simulate a setting with  $P = 100$  distributed nodes, where the underlying signal is Bernoulli Gaussian (5) of length  $N = 20,000$  with sparsity rate  $\epsilon = 0.1$ . We constrain the algorithm to have no more than 10 MP-AMP iterations, and the aggregate coding rate is  $R_{agg} = 20$  bits. We test 9 different measurement rates from 0.2 to 0.6 and 4 different SNR's from 5 dB to 20 dB.

We call the SDR at the last MP-AMP iteration the *final SDR*. The final SDR's from DP prediction and MP-AMP simulation, along with the SDR corresponding to the MMSE [18, 19], are shown in Fig. 5(a) as a function of the measurement rate  $\kappa$ . We can see that all MP-AMP results match the DP prediction. In settings with low SNR or high measurement rate  $\kappa$ , MP-AMP achieves the MMSE with an aggregate coding rate of only  $R_{agg} = 20$  bits (4). In contrast, conventional floating point schemes need 32 bits per entry per iteration for single precision, resulting in  $R_{agg} = 320$  bits. However, in many cases  $R_{agg} = 320$  bits only achieves marginally (less than 1 dB) better SDR than the coding rate sequence with  $R_{agg} = 20$  bits given by DP. Hence,  $R_{agg} = 20$  bits offers a dramatic

reduction in the communication cost, while the difference in the final SDR is modest.

Another interesting aspect of Fig. 5(a) is that MP-AMP results are several dB worse than the MMSE in settings with low measurement rate  $\kappa$  and high SNR. This underperformance is due to the insufficient aggregate coding rate  $R_{agg}$  (4). In order to verify that larger aggregate coding rates help the MSE of the DP scheme approach the MMSE, we run DP with  $R_{agg} = 30, 60$ , and 80 bits without constraining  $T$ ,<sup>7</sup> and obtain the results shown in Fig. 5(b). We can see for SNR=10 dB that  $R_{agg} = 30$  bits yields a final SDR that is close to the MMSE;  $R_{agg} = 60$  bits is needed for SNR=15 dB and  $R_{agg} = 80$  bits for SNR=20 dB, except for the case with  $\kappa = 0.25$ , which needs larger aggregate coding rate  $R_{agg}$ .

**Remark:** Examining all coding rate sequences  $(R_t)$  in our DP results, we notice that the coding rate is monotone non-decreasing, i.e.,  $R_1 \leq R_2 \leq \dots \leq R_T$ . This seems intuitive, because in early iterations of (MP-)AMP, the scalar channel noise  $\mathbf{w}_t^p$  is large, which does not require transmitting high fidelity  $\mathbf{f}_t^p$  (cf. (17)). Hence, low rate  $R_t$  is good enough. As the iterations proceed, the scalar channel noise  $\mathbf{w}_t^p$  is reduced, and large quantization error  $\mathbf{n}_t^p$  (17) will be unfavorable to the final SDR. Hence, higher rates are needed in later iterations.

## VI. REAL-WORLD CASE STUDY

In the DP formulation of Sec. III, we found the coding rate sequence  $(R_t)$  that yields the lowest MSE given a certain rate budget  $R_{agg}$  (4) and  $T$  MP-AMP iterations. In some applications (see below), we may want to obtain a sufficiently small MSE at minimum *cost*, where the physical meaning of the cost varies in different problems. We discuss two MP platforms, sensor networks [20, 21] and large-scale cloud servers [22]. The costs in these two platforms are quite different due to the different constraints in these platforms, and we will see how they affect the optimal coding rate sequence  $(R_t)$ . The change in the optimal  $(R_t)$  highlights the importance of optimizing for the correct costs.

### A. Sensor networks

In sensor networks [20, 21], distributed sensors are typically dispatched to remote locations where they collect data and communicate with the fusion center. However, distributed sensors may have severe power consumption constraints. Therefore, low power chips such as the CC253X from Texas Instruments [23] are commonly used in distributed sensors. Some typical parameters for such low power chips are: central processing unit (CPU) clock frequency 32MHz, data transmission rate 250Kbps, voltage between 2V-3.6V, and transceiver current 25mA [23], where the CPU current resembles the transceiver current. Because these chips are generally designed to be low power, when transmitting and receiving data, the CPU helps the transceiver and cannot carry out computing tasks at the same time. Therefore, the power consumption can be viewed as constant. Hence, in order to minimize the power consumption cost, we minimize the total runtime

<sup>6</sup>More precise characterizations of the MMSE appear in Krzakala et. al. [18, 19] and Zhu and Baron [17].

<sup>7</sup>Unconstrained  $T$  can be accomplished by supplying a large enough  $T$ , in which case DP will assign  $R_t = 0$  in the first several MP-AMP iterations.

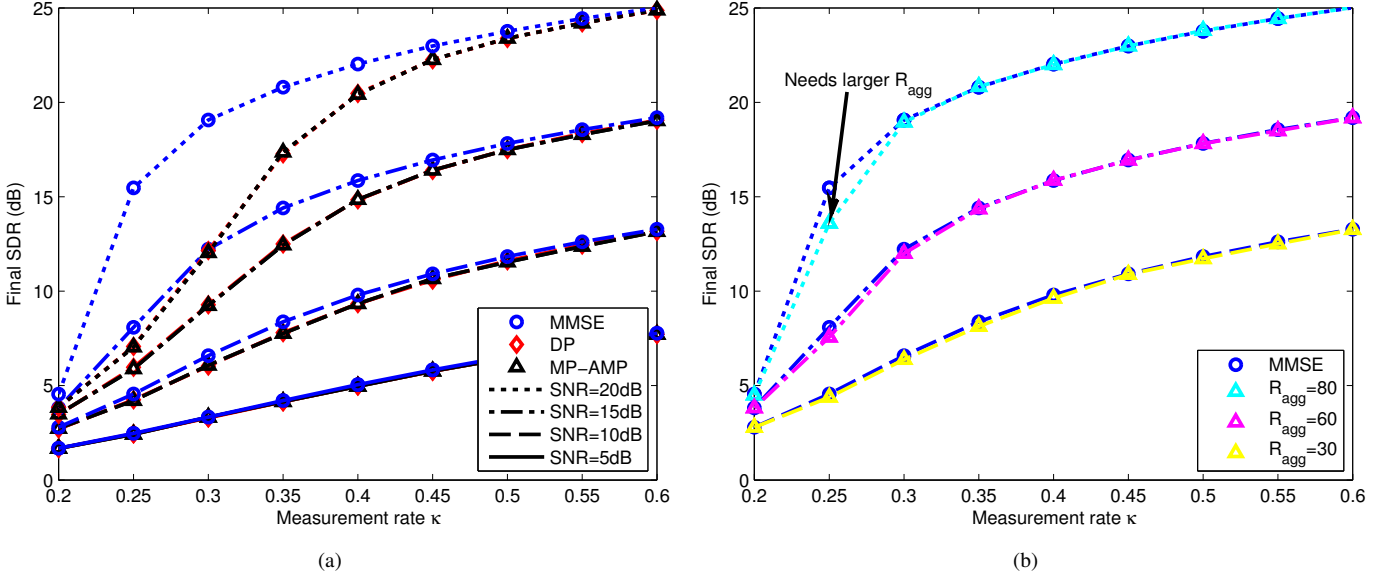


Fig. 5. Final SDR's corresponding to the MMSE, DP prediction, and MP-AMP simulation as a function of measurement rate  $\kappa$  and SNR: (a) DP is constrained to 10 MP-AMP iterations and aggregate coding rate  $R_{agg} = 20$  bits (4) and (b) no constraint on iterations  $T$  and larger rates  $R_{agg}$ .

when reconstructing a signal from MP-CS measurements (2) collected by the distributed sensors.

The runtime in each MP-AMP iteration (12)-(16) consists of (i) time for computing (12) and (13), (ii) time for encoding  $\mathbf{f}_t^p$  (13), and (iii) data transmission time for  $Q(\mathbf{f}_t^p)$  (17). As discussed in Sec. II-B, the downlink may broadcast  $\mathbf{x}_t$  (16), and simple compression schemes can reduce the coding rate. Therefore, we consider the data reception time in the downlink to be constant. The overall computational complexity for (12) and (13) is  $\mathcal{O}(\frac{MN}{P})$ . Considering the overhead of moving data in memory, together with the clock frequency being 32MHz, we assume that the actual time needed for computing (12) and (13) is  $C_1 = \frac{20MN}{32 \times 10^6 P}$  sec. Transmitting  $Q(\mathbf{f}_t^p)$  of length  $N$  at coding rate  $R$  requires  $\frac{RN}{250 \times 10^3}$  sec, where the denominator is the data transmission rate of the transceiver. Considering other overheads, we assume that the time requested for transmitting  $Q(\mathbf{f}_t^p)$  at coding rate  $R$  is  $C_2 R$  sec, where  $C_2 = \frac{2N}{250 \times 10^3}$ . Therefore, the total cost is

$$\Psi = \sum_{t=1}^T (C_1 \times \mathbb{1}_{R_t \neq 0} + C_2 R_t), \quad (26)$$

where  $R_t$  is the coding rate for MP-AMP iteration  $t$  and  $\mathbb{1}_{\mathcal{A}}$  is the indicator function, which is 1 if the condition  $\mathcal{A}$  is met, else 0. To find the coding rate sequence  $(R_t)$  that minimizes the cost function in (26), we design unconstrained DP.

### B. Unconstrained DP

Our goal is to find a coding rate sequence  $(R_t)$  for each MP-AMP iteration such that the final MSE is within  $\Delta$  dB of the MMSE, while achieving the minimum cost  $\Psi$ . More specifically, the aggregate coding rate  $R_{agg}$  (4) and total number of iterations  $T$  are not constrained. To do so, we modify the DP scheme of Sec. III, and obtain the following unconstrained DP, which can be used to solve this problem.

The cost  $\Psi$  is a function of the number of remaining iterations  $(T-t)$  and the current scalar channel noise variance  $\sigma_t^2$  (19). In the basis case  $T-t=0$ , the cost is  $C_1 + C_2 R_T$ . With  $C_1$  being fixed, among values of  $R$  that yield small enough error, the smallest  $R$  has the lowest cost. If  $\sigma_T^2$  is too large, even lossless transmission of  $\mathbf{f}_T^p$  during the single remaining MP-AMP iteration (21) does not yield an MSE within  $\Delta$  dB of the MMSE. Therefore, we assign  $\Psi_0(\sigma_T^2) = \infty$  for such  $\sigma_T^2$ . Next, we iterate back in time by decreasing  $t$  (equivalently, increasing  $T-t$ ),

$$\Psi_{T-t}(\sigma_t^2) = \min_{R'} \{C_1 \times \mathbb{1}_{R' \neq 0} + C_2 R' + \Psi_{T-(t+1)}(\sigma_{t+1}^2(R'))\},$$

where  $R'$  is the coding rate used in the current MP-AMP iteration  $t$ , and  $\sigma_{t+1}^2(R')$  is the variance of the noise  $\mathbf{w}_{t+1}$  of the scalar channel (19) in the next MP-AMP iteration after transmitting  $\mathbf{f}_t^p$  at rate  $R'$ . The terms on the right hand side are the computational cost, communication cost, and the minimum combined cost in all latter iterations,  $t+1, \dots, T$ , given  $R'$  being used in the current iteration  $t$  with the equivalent scalar channel noise variance at the fusion center being  $\sigma_t^2$  (19). As in Sec. III, a discretized search space is utilized. However, it is important to use a finer search grid (we use  $\Delta\sigma_t^2 = 0.01$  dB) to support larger coding rates, which are required because the unconstrained optimization is more sensitive to  $\sigma_t^2$  at high rates (21). This section uses the RD function  $R(D)$  [24–26] to model the relation between rate and distortion.

The coding rates  $R'$  that minimize the cost function  $\Psi_{T-t}(\sigma_t^2)$  for different  $t$  and  $\sigma_t^2$  are stored in a table  $\mathcal{R}(t, \sigma_t^2)$ . Having computed  $\mathcal{R}(t, \sigma_t^2)$ , the coding rate sequence is obtained as in Sec. III.

Now that unconstrained DP is developed, we use it to find the coding rate sequence  $(R_t)$  that minimizes the cost (26) for sensor networks. Because low power chips equipped in distributed sensors have limited memory (around 10KB, al-



though sometimes external flash is allowed) [23], the signal length  $N$  and number of measurements  $M$  cannot be too large. We consider  $N = 1,000$  and  $M = 400$  spread over  $P = 100$  sensors, sparsity rate  $\epsilon = 0.1$ , and  $\text{SNR} = 20$  dB. We set  $\Delta = 0.5$  dB and run unconstrained DP. The coding rate sequence provided by unconstrained DP is  $(R_t) = (0.1, 0.1, 0.6, 0.8, 1.0, 1.0, 1.1, 1.1, 1.2, 1.4, 1.6, 1.9, 2.3, 2.7, 3.1)$ , where the first and last numbers in  $(R_t)$  are coding rates corresponding to the first and last iterations, respectively. In total we have  $T = 15$  MP-AMP iterations with  $R_{agg} = 20.0$  bits aggregate coding rate (4). The DP-predicted SDR (25) is 21.52 dB, which is within  $\Delta = 0.5$  dB of the SDR for the MMSE (22.02 dB) [17–19]. The total cost is verified to be optimal by the same techniques discussed in the Appendix.

### C. Large-scale cloud server

Having discussed sensor networks [20, 21], we now discuss an application of unconstrained DP (cf. Sec. VI-B) to large-scale cloud servers. Consider the dollar cost for users of Amazon EC2 [22], a commercial cloud computing service. A typical cost for CPU time is \$0.03/hour, and the data transmission cost is \$0.03/GB. Assuming that the CPU clock frequency is 2.0GHz and considering various overheads, we need a runtime of  $\frac{20MN}{2 \times 10^9 P}$  sec and the computation cost is  $\$ \frac{20MN}{2 \times 10^9 P} \times \frac{0.03}{3600}$  per MP-AMP iteration. Similar to Sec. VI-A, the communication cost for coding rate  $R$  is  $\$ 2RN \frac{0.03}{8 \times 10^9}$ . Therefore, the total cost with  $T$  MP-AMP iterations can still be modeled as in (26), where  $C_1 = \frac{20MN}{2 \times 10^9 P} \times \frac{0.03}{3600}$  and  $C_2 = 2RN \frac{0.03}{8 \times 10^9}$ .

We consider a problem with the same signal and channel model as the setting of Sec. VI-A, while the size of the problem grows to  $N = 50,000$  and  $M = 20,000$  spread over  $P = 100$  computing nodes. Running the unconstrained DP, we obtain the coding rate sequence  $(R_t) = (1.3, 1.6, 1.8, 1.8, 1.8, 1.9, 2.1, 2.3, 2.6, 3.1, 3.7)$  for a total of  $T = 11$  MP-AMP iterations with  $R_{agg} = 24.0$  bits aggregate coding rate. The DP-predicted SDR (25) is 21.53 dB, which is within  $\Delta = 0.5$  dB of the SDR for the MMSE (this result is 0.01 dB better than that for sensor networks in Sec. VI-B due to the finite resolution of our grid). The total cost is verified to be optimal by the same techniques discussed in the Appendix.

**Settings with even cheaper communication costs:** The reader can see that the actual cost depends on the two constants,  $C_1$  and  $C_2$ , which correspond to computation and communication, respectively. Suppose that the relative cost of communication, compared to computation, is even cheaper than above, which is true for multi-processor CPU or graphics processing unit (GPU) systems. We keep  $C_1$  the same as above, and reduce  $C_2$  by a factor of 100. We run the unconstrained DP again, and obtain the following coding rate sequence  $(R_t) = (2.3, 2.5, 2.6, 2.7, 2.7, 2.8, 3.0, 3.4, 3.7, 4.5)$  for  $T = 10$  and  $R_{agg} = 30.2$  bits. Note that 10 iterations are needed for centralized AMP to converge in this setting. With the low-cost communication of this setting, DP yields a coding rate sequence  $(R_t)$  within 0.5 dB of the MMSE with the same number of iterations as centralized AMP, while using an average coding rate of only 3.02 bits per iteration.

### D. Pareto optimality study

So far, we have seen in Sec. VI that the constants  $C_1$  and  $C_2$  model the constraints of the system, and affect the optimal number of iterations  $T$  and the optimal aggregate coding rate  $R_{agg}$  (4). In reality, there is a trade-off between  $T$  and  $R_{agg}$ , and there is no optimal solution that minimizes them simultaneously. To deal with such trade-offs in a multi-objective optimization (MOP) problem, it is customary to think about the concept of *Pareto optimality* [39].

For notational convenience, define the excess MSE,

$$\text{EMSE}_{\text{db}} := 10 \log_{10}(\text{MSE}(T, R_{agg})/\text{MMSE}), \quad (27)$$

with  $\text{MSE}(T, R_{agg})$  denoting the smallest MSE that the pair  $(T, R_{agg})$  can provide under the constraint  $b = \frac{C_1}{C_2} \in [0, \infty)$ . Furthermore, let

$$\mathcal{C} = \{(T, R_{agg}) : (T, R_{agg}) \in \mathbb{R}^+ \times \mathbb{R}^+, \text{EMSE}_{\text{db}} \leq \Delta\}.$$

*Definition 1:* The point  $\mathcal{X}_1 \in \mathcal{C}$  is said to dominate another point  $\mathcal{X}_2 \in \mathcal{C}$ , denoted by  $\mathcal{X}_1 \prec \mathcal{X}_2$ , if and only if  $T_1 \leq T_2$  and  $R_{agg1} \leq R_{agg2}$ . A point  $\mathcal{X}^* \in \mathcal{C}$  is said to be Pareto optimal if and only if there does not exist  $\mathcal{X} \in \mathcal{C}$  satisfying  $\mathcal{X} \prec \mathcal{X}^*$ . Furthermore, let  $\mathcal{P}$  denote the set of all Pareto optimal points,

$$\mathcal{P} := \{\mathcal{X} \in \mathcal{C} : \mathcal{X} \text{ is Pareto optimal}\}.$$

In words, the pair  $(T, R_{agg})$  is Pareto optimal if no other pair  $(T', R'_{agg})$  exists such that  $T' \leq T$  and  $R'_{agg} \leq R_{agg}$ .

In this section, we extend the definition of the number of iterations to a probabilistic one. We assume that the number of iterations is drawn from a probability distribution  $\pi$  over  $\mathbb{N}$ , such that  $\sum_{i=1}^{\infty} \pi_i = 1$ . Of course, this definition contains a deterministic  $T = j$  as a special case with  $\pi_j = 1$  and  $\pi_i = 0$  for all  $i \neq j$ . We further define the function  $\underline{R}(\cdot) : (1, \infty) \rightarrow \mathbb{R}^+$  as the Pareto optimal function implicitly as follows:

$$\underline{R}(T) = R_{agg} \Leftrightarrow (T, R_{agg}) \in \mathcal{P}.$$

Armed with this definition of Pareto optimality and the probabilistic definition of the number of iterations, we have the following lemma.

*Lemma 1:* For a fixed noise variance  $\sigma_Z^2$ , measurement rate  $\kappa$ , optimality gap  $\Delta$ , and  $P$  distributed nodes in MP-AMP, the Pareto optimal function  $\underline{R}(\cdot)$  is a convex function of  $T$ .

*Proof:* First, we show that it suffices to show that for any  $(T^{(1)}, R_{agg}^{(1)}), (T^{(2)}, R_{agg}^{(2)}) \in \mathcal{C}$  and any  $0 < \lambda < 1$ ,

$$(\lambda T^{(1)} + (1 - \lambda)T^{(2)}, \lambda R_{agg}^{(1)} + (1 - \lambda)R_{agg}^{(2)}) \in \mathcal{C}. \quad (28)$$

If (28) holds, we could pick the pairs  $(T^{(1)}, R_{agg}^{(1)}), (T^{(2)}, R_{agg}^{(2)}) \in \mathcal{P}$  on the Pareto optimal curve, implying that  $\underline{R}(T^{(1)}) = R_{agg}^{(1)}$ ,  $\underline{R}(T^{(2)}) = R_{agg}^{(2)}$ , and

$$\begin{aligned} \underline{R}(\lambda T^{(1)} + (1 - \lambda)T^{(2)}) &\leq \lambda R_{agg}^{(1)} + (1 - \lambda)R_{agg}^{(2)} \\ &= \lambda \underline{R}(T^{(1)}) + (1 - \lambda)\underline{R}(T^{(2)}), \end{aligned}$$

which proves convexity.

To show (28), we use the well-known time-sharing argument (see [25]). Assume that  $(T^{(1)}, R_{agg}^{(1)}), (T^{(2)}, R_{agg}^{(2)}) \in \mathcal{C}$  are achieved by probability distributions  $\pi^{(1)}$  and  $\pi^{(2)}$ , respectively. Let us pick all the parameters of the first pair with probability  $\lambda$  and those of the second pair with probability

$(1-\lambda)$ . Hence, we have  $\pi = \lambda\pi^{(1)} + (1-\lambda)\pi^{(2)}$ , and due to the linearity of expectation,  $T = \lambda T^{(1)} + (1-\lambda)T^{(2)}$ . Again, due to the linearity of expectation,  $R_{agg} = \lambda R_{agg}^{(1)} + (1-\lambda)R_{agg}^{(2)}$ , and the EMSE<sub>db</sub> constraint (27) is satisfied by both pairs, implying that (28) is satisfied, and the proof is complete. ■

In our experiments, we test a variety of ratios  $b = \frac{C_1}{C_2}$  for three different thresholds,  $\Delta \in \{0.3, 0.5, 1.0\}$  dB. According to Definition 1, the resulting aggregate coding rates  $R_{agg}$  (4) and numbers of iterations  $T$  from unconstrained DP are Pareto optimal, and are plotted in Fig. 1 for different  $\Delta$ . The curves in Fig. 1 are convex, as implied by Lemma 1. Also, with stricter requirements on the final SDR (25) (meaning smaller  $\Delta$ ), more iterations  $T$  and greater aggregate coding rates  $R_{agg}$  (4) are needed. Optimal coding rate sequences spend more coding rate to reduce the number of iterations when communication costs are low, whereas more iterations allow to reduce the coding rate when communication is costly.

## VII. CONCLUSION

This paper used lossy compression in multi-processor (MP) approximate message passing (AMP) for solving MP compressed sensing problems. The trade-off between rate and distortion of the lossy compression was modeled by both the theoretic rate distortion (RD) function and scalar quantization with entropy coding (ECSQ). Dynamic programming (DP) was used to find the optimal coding rate sequence in each MP-AMP iteration in order to provide the lowest mean squared error or the lowest customized cost in MP computing platforms. We verified that MP-AMP simulation results achieve the signal-to-distortion performance predicted by DP.

To the best of our knowledge, this is the first work that brings together RD theory, AMP, distributed computing, and DP.<sup>8</sup> In existing MP platforms, the data must be transmitted at full precision, which is unnecessary. This work presents opportunities for lossy compression to reduce communication costs in large-scale MP platforms. At the same time, many topics remain to be explored. For example, this work only optimized the lossy compression used in the uplink, while the downlink was not discussed. If the downlink uses lossy compression, the SE needs to be modified accordingly to accommodate the quantization error from the uplink. A second topic would be to study vector quantization (VQ) schemes that are suitable for distributed computing. Designing a VQ scheme is not straightforward, because VQ requires searching through a codebook whose size increases exponentially with the block length, which will increase the computational burden. The complex nature of VQ design raises the following question: what is the best trade-off among various possible block lengths, various quantization qualities, and the computational requirements? We believe that this can be an interesting optimization area to study.

## ACKNOWLEDGMENTS

The authors thank Puxiao Han and Ruixin Niu for numerous discussions about MP settings of CS and AMP; Ahmad

Beirami shared insights on lossy compression and Pareto optimality; and Mohsen Sardari and Mihail Sichitiu offered useful information about the practical distributed computing platforms of Sec. VI. Finally, we thank Yanting Ma and Ryan Pilgrim for helpful comments about the manuscript.

## APPENDIX

**Integrity of discretized search space:** When a coding rate  $R'$  is selected in MP-AMP iteration  $t$ , DP calculates the equivalent scalar channel noise variance  $\sigma_{t+1}^2$  (19) for the next MP-AMP iteration according to (21). The variance  $\sigma_{t+1}^2$  is unlikely to lie on the discretized grid  $\mathcal{G}(\sigma^2)$ . Therefore,  $\Psi_{T-(t+1)}(R_{rem}(t+1), \sigma_{t+1}^2)$  does not reside in memory, where  $R_{rem}(t+1) = R_{rem}(t) - R'$  (23). Instead of brute-force calculation of  $\Psi_{\{\cdot\}}(\cdot, \sigma_{t+1}^2)$ , we estimate it by fitting a function to the closest neighbors of  $\sigma_{t+1}^2$  that lie on the grid  $\mathcal{G}(\sigma^2)$  for arbitrary fixed  $R_{rem}(t+1)$  and  $t+1$ , and finding  $\Psi_{\{\cdot\}}(\cdot, \sigma_{t+1}^2)$  according to the fit function. We evaluate two *interpolation* schemes, linear interpolation and quadratic interpolation.

*Interpolation in  $\mathcal{G}(\sigma^2)$ :* We run DP over the original coarse grid  $\mathcal{G}^c(\sigma^2)$  with resolution  $\Delta\sigma^2 = 0.1$  dB, and a  $4\times$  finer grid  $\mathcal{G}^f(\sigma^2)$  with  $\Delta\sigma^2 = 0.025$  dB. We obtain the cost function with the coarse grid  $\Psi_{T-t}^c(R, \sigma_c^2)$  and the cost function with the fine grid  $\Psi_{T-t}^f(R, \sigma_f^2)$ ,  $\forall R \in \mathcal{G}(R), t \in \{1, \dots, T\}, \sigma_c^2 \in \mathcal{G}^c(\sigma^2), \sigma_f^2 \in \mathcal{G}^f(\sigma^2)$ . Next, we interpolate  $\Psi_{T-t}^c(\cdot, \cdot)$  over the fine grid  $\mathcal{G}^f(\sigma^2)$  and obtain the interpolated  $\Psi_{T-t}^i(\cdot, \cdot)$ . By comparing  $\Psi_{T-t}^i(\cdot, \cdot)$  to  $\Psi_{T-t}^f(\cdot, \cdot)$ , we verify that linear interpolation is faster but somewhat less accurate than quadratic interpolation. Nevertheless, linear interpolation comes within 0.01 dB of quadratic interpolation,<sup>9</sup> and we feel that the speed of linear interpolation justifies this minor decrease in precision. Therefore, we use linear interpolation with a coarse grid  $\mathcal{G}^c(\sigma^2)$  with  $\Delta\sigma^2 = 0.1$  dB.

*Integrity of choice of  $\Delta R$ :* We tentatively select resolution  $\Delta R = 0.1$ , and investigate the integrity of this  $\Delta R$  over the 64 different settings from Sec. IV. After the coding rate sequence  $(R_t)$  is obtained by DP for each setting, we randomly perturb  $R_t$  by  $R_p(t) = R_t + \beta_t$ ,  $t = 1, \dots, T$ , where  $R_p(t)$  is the *perturbed coding rate*, the bias is  $\beta_t \in [-\frac{\Delta R}{2}, +\frac{\Delta R}{2}]$ , and  $(R_p(t))$ ,  $t = 1, \dots, T$ , is called the *perturbed coding rate sequence*. We constrain the perturbed coding rates to satisfy  $R_p(t) \geq 0$ ,  $t = 1, \dots, T$ , with  $\sum_{t=1}^T R_p(t) = R_{agg}$ . After randomly generating 100 different perturbed coding rate sequences  $(R_p(t))$ , we calculate the DP-predicted SDR for each  $(R_p(t))$ . Fig. 6(a) plots the sorted SDR difference,  $\Delta\text{SDR} = \text{SDR}_p - \text{SDR}_o$ , where  $\text{SDR}_p$  and  $\text{SDR}_o$  are the final SDR's for the perturbed and original coding rate sequences, respectively. We can see that  $\Delta R = 0.1$  yields probability  $\Pr(\Delta\text{SDR} < 0.001) > 95\%$ , which means that with high probability the coding rate sequence obtained by DP with  $\Delta R = 0.1$  will be negative (and thus optimal) or marginally suboptimal. Hence, we verified the integrity of  $\Delta R = 0.1$ .

**Verification of DP optimality:** In order to verify that DP computes the optimal coding rate sequence using the current

<sup>8</sup>A subset of the work with Puxiao Han and Ruixin Niu will appear at the 41st IEEE International Conference on Acoustics, Speech and Signal Processing, Shanghai, China, Mar. 2016 [1].

<sup>9</sup>Note that when calculating  $\Psi^f$ , we are still using the corresponding interpolation scheme. Although this comparison is not ideal, we believe it still provides the reader with enough insight.

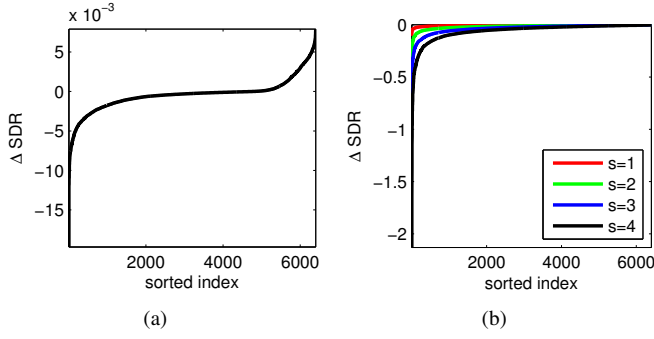


Fig. 6. SDR difference for the perturbed coding rate sequence ( $R_p(t)$ ): (a) perturbation within resolution  $\Delta R$  of the coding rate sequence ( $R_t$ ) obtained by DP using the RD function and (b) perturbation on the grid  $\mathcal{G}(R)$  of the coding rate sequence obtained by DP using the RD function.

discrete search grid for  $R$ , we run DP using the 64 different settings from Sec. IV. After the coding rate sequence ( $R_t$ ) is obtained for each setting, we randomly perturb  $R_t$  by  $R_p(t) = R_t + \beta_t^s$ ,  $t = 1, \dots, T$ , where  $\beta_t^s \in \{-s, -s+1, \dots, +s\}$  for fixed  $s$ . We randomly generate 100 different perturbed coding rate sequences ( $R_p(t)$ ) while constraining the perturbed coding rates  $R_p(t) \geq 0$ ,  $t = 1, \dots, T$ , and  $\sum_{t=1}^T R_p(t) = R_{agg}$  for each  $s \in \{1, 2, 3, 4\}$ , and plot the sorted SDR difference in Fig. 6(b). We can see that larger perturbations will make the DP-predicted SDR (25) smaller (hence, larger MSE).<sup>10</sup> Therefore, we verified that the coding rate sequences obtained by our DP scheme are optimal.

## REFERENCES

- [1] P. Han, J. Zhu, R. Niu, and D. Baron, "Multi-processor approximate message passing using lossy compression," in *IEEE Int. Conf. Acoustics, Speech, Signal Process. (ICASSP)*, Shanghai, China, Mar. 2016.
- [2] D. Donoho, "Compressed sensing," *IEEE Trans. Inf. Theory*, vol. 52, no. 4, pp. 1289–1306, Apr. 2006.
- [3] E. Candès, J. Romberg, and T. Tao, "Robust uncertainty principles: Exact signal reconstruction from highly incomplete frequency information," *IEEE Trans. Inf. Theory*, vol. 52, no. 2, pp. 489–509, Feb. 2006.
- [4] J. Mota, J. Xavier, and P. Aguiar, "Distributed basis pursuit," *IEEE Trans. Signal Process.*, vol. 60, no. 4, pp. 1942–1956, Apr. 2012.
- [5] S. Patterson, Y. C. Eldar, and I. Keidar, "Distributed sparse signal recovery for sensor networks," in *IEEE Int. Conf. Acoustics, Speech, Signal Process. (ICASSP)*, Vancouver, BC, Canada, May 2013, pp. 4494–4498.
- [6] S. Patterson, Y. C. Eldar, and I. Keidar, "Distributed compressed sensing for static and time-varying networks," *IEEE Trans. Signal Proc.*, vol. 62, no. 19, pp. 4931–4946, Oct. 2014.
- [7] P. Han, R. Niu, M. Ren, and Y. C. Eldar, "Distributed approximate message passing for sparse signal recovery," in *Proc. IEEE Global Conf. Signal Inf. Process.*, Atlanta, GA, Dec. 2014, pp. 497–501.
- [8] P. Han, R. Niu, and Y. C. Eldar, "Modified distributed iterative hard thresholding," in *IEEE Int. Conf. Acoustics, Speech, Signal Process. (ICASSP)*, Brisbane, Australia, Apr. 2015, pp. 3766–3770.
- [9] C. Ravazzi, S. M. Fossion, and E. Magli, "Distributed iterative thresholding for  $\ell_0/\ell_1$ -regularized linear inverse problems," *IEEE Trans. Inf. Theory*, vol. 61, no. 4, pp. 2081–2100, Apr. 2015.
- [10] P. Han, R. Niu, and Y. C. Eldar, "Communication-efficient distributed IHT," in *Proc. Signal Processing with Adaptive Sparse Structured Representations Workshop (SPARS)*, Cambridge, United Kingdom, July 2015.
- [11] D. L. Donoho, A. Maleki, and A. Montanari, "Message passing algorithms for compressed sensing," *Proc. Nat. Academy Sci.*, vol. 106, no. 45, pp. 18914–18919, Nov. 2009.
- [12] A. Montanari, "Graphical models concepts in compressed sensing," *Compressed Sensing: Theory and Applications*, pp. 394–438, 2012.
- [13] M. Bayati and A. Montanari, "The dynamics of message passing on dense graphs, with applications to compressed sensing," *IEEE Trans. Inf. Theory*, vol. 57, no. 2, pp. 764–785, Feb. 2011.
- [14] T. Tanaka, "A statistical-mechanics approach to large-system analysis of CDMA multiuser detectors," *IEEE Trans. Inf. Theory*, vol. 48, no. 11, pp. 2888–2910, Nov. 2002.
- [15] D. Guo and S. Verdú, "Randomly spread CDMA: Asymptotics via statistical physics," *IEEE Trans. Inf. Theory*, vol. 51, no. 6, pp. 1983–2010, June 2005.
- [16] D. Guo and C. C. Wang, "Multiuser detection of sparsely spread CDMA," *IEEE J. Select. Areas Commun.*, vol. 26, no. 3, pp. 421–431, Apr. 2008.
- [17] J. Zhu and D. Baron, "Performance regions in compressed sensing from noisy measurements," in *Proc. 2013 Conf. Inference Sci. Syst. (CISS)*, Baltimore, MD, Mar. 2013.
- [18] F. Krzakala, M. Mézard, F. Sausset, Y. Sun, and L. Zdeborová, "Probabilistic reconstruction in compressed sensing: Algorithms, phase diagrams, and threshold achieving matrices," *J. Stat. Mech. - Theory E*, vol. 2012, no. 08, pp. P08009, Aug. 2012.
- [19] F. Krzakala, M. Mézard, F. Sausset, Y. Sun, and L. Zdeborová, "Statistical-physics-based reconstruction in compressed sensing," *Phys. Rev. X*, vol. 2, no. 2, pp. 021005, May 2012.
- [20] G. J. Pottie and W. J. Kaiser, "Wireless integrated network sensors," *Commun. ACM*, vol. 43, no. 5, pp. 51–58, May 2000.
- [21] D. Estrin, D. Culler, K. Pister, and G. Sukhatme, "Connecting the physical world with pervasive networks," *IEEE Pervasive Comput.*, vol. 1, no. 1, pp. 59–69, Jan. 2002.
- [22] "Amazon EC2," <https://aws.amazon.com/ec2/>.
- [23] Texas Instruments, *A True System-on-Chip Solution for 2.4-GHz IEEE 802.15.4 and ZigBee Applications*, Apr. 2009, Rev. B.
- [24] T. Berger, *Rate distortion theory: a mathematical basis for data compression*, Prentice-Hall Englewood Cliffs, NJ, 1971.
- [25] T. M. Cover and J. A. Thomas, *Elements of Information Theory*, New York, NY, USA: Wiley-Interscience, 2006.
- [26] A. Gersho and R. M. Gray, *Vector quantization and signal compression*, Kluwer, 1993.
- [27] D. P. Bertsekas, *Dynamic programming and optimal control*, vol. 1, Athena Scientific Belmont, MA, 1995.
- [28] S. Arimoto, "An algorithm for calculating the capacity of an arbitrary discrete memoryless channel," *IEEE Trans. Inf. Theory*, vol. 18, pp. 14–20, Jan. 1972.
- [29] R. E. Blahut, "Computation of channel capacity and rate-distortion functions," *IEEE Trans. Inf. Theory*, vol. 18, no. 4, pp. 460–473, July 1972.
- [30] K. Rose, "A mapping approach to rate-distortion computation and analysis," *IEEE Trans. Inf. Theory*, vol. 40, no. 6, pp. 1939–1952, Nov. 1994.
- [31] Y. Linde, A. Buzo, and R. M. Gray, "An algorithm for vector quantizer design," *IEEE Trans. Comm.*, vol. 28, no. 1, pp. 84–95, Jan. 1980.
- [32] R. M. Gray, "Vector quantization," *IEEE ASSP Magazine*, vol. 1, no. 2, pp. 4–29, Apr. 1984.
- [33] D. Guo and C. Wang, "Asymptotic mean-square optimality of belief propagation for sparse linear systems," in *IEEE Inf. Theory Workshop*, Oct. 2006, pp. 194–198.
- [34] S. B. Korada and R. L. Urbanke, "Polar codes are optimal for lossy source coding," *IEEE Trans. Inf. Theory*, vol. 56, no. 4, pp. 1751–1768, Apr. 2010.
- [35] D. Guo, D. Baron, and S. Shamai, "A single-letter characterization of optimal noisy compressed sensing," in *Proc. 47th Allerton Conf. Commun., Control, and Comput.*, Sept. 2009, pp. 52–59.
- [36] S. Rangan, A.K. Fletcher, V.K. Goyal, and P. Schniter, "Hybrid approximate message passing with applications to structured sparsity," *Arxiv preprint arXiv:1111.2581*, Nov. 2011.
- [37] Y. Ma, D. Baron, and A. Beirami, "Mismatched estimation in large linear systems," in *Proc. IEEE Int. Symp. Inf. Theory (ISIT)*, July 2015.
- [38] B. Widrow and I. Kollár, *Quantization Noise: Roundoff Error in Digital Computation, Signal Processing, Control, and Communications*, Cambridge University press, 2008.
- [39] I. Das and J. E. Dennis, "Normal-boundary intersection: A new method for generating the Pareto surface in nonlinear multicriteria optimization problems," *SIAM J. Optimization*, vol. 8, no. 3, pp. 631–657, Aug. 1998.

<sup>10</sup>There are a few cases where the perturbed sequences are slightly better than the DP results due to floating point precision, which can be ignored.